analytical chemistry

Article

pubs.acs.org/ac

Reusable and Dual-Potential Responses Electrogenerated Chemiluminescence Biosensor for Synchronously Cytosensing and Dynamic Cell Surface N-Glycan Evaluation

Yao He, Jinghong Li, and Yang Liu*

Department of Chemistry, Beijing Key Laboratory for Analytical Methods and Instrumentation, Tsinghua University, Beijing 100084, China

Supporting Information

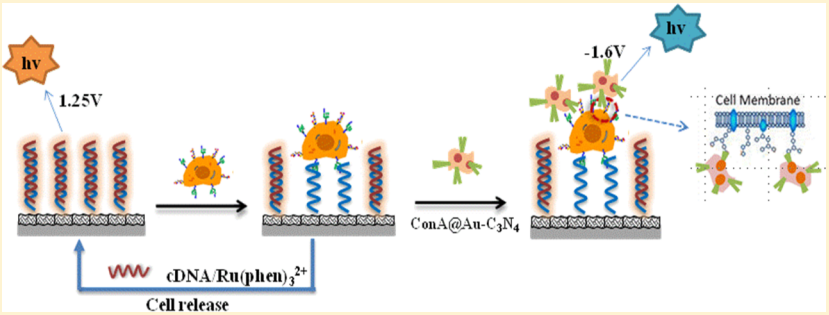

ABSTRACT: A novel reusable and dual-potential responsive electrogenerated chemiluminescence (ECL) biosensor was fabricated for synchronous detection of cancer cells and their surface N-glycan. In this strategy, a cancer cell recognized aptamer hybridized with a capture DNA was immobilized on electrochemically reduced MoS_2 nanosheets, and Ru(phen)$_3^{2+}$ as ECL probes was intercalated into the grooves of the double-strand DNA. In the presence of target cells, the capture DNA and Ru(phen)$_3^{2+}$ were released from the electrode interface owing to the specific interaction between cancer cells and the aptamer. Meanwhile, concanavalin A (Con A), a mannose binding protein, and a conjugated gold nanoparticle modified graphite-C_3N_4 (Con A@Au-C_3N_4) was used as a negative ECL nanoprobe and applied for the cell surface N-glycan evaluation owing to the excellent ECL properties of g-C_3N_4 at negative potential. The cytosensing and cell surface N-glycan evaluation could be simultaneously realized with high sensitivity and excellent selectivity based on the ratio of ECL intensity between the negative potential and positive potential ($\Delta ECL_n/\Delta ECL_p$), avoiding the traditional routing cell counting procedures. Moreover, the aptamer modified electrode can be regenerated in the presence of capture DNA solutions for cyclic utilization. As a proof-of-concept, the ECL cytosensor showed excellent performances for the analysis of the MCF-7 cancer cell and its surface N-glycan evaluation in human serum samples. The reusable and dual potential response ECL biosensor endows a feasibility tool for clinical diagnosis and drug screening especially in complex biological systems.

Cell surface glycoproteins and glycolipids play crucial roles in cell communication and differentiation, signaling, immunological recognition, and metastasis among other processes.[1−7] Glycan epitopes are generally the surface markers to detect and recognize specific types of cells, such as tumor cells and stem cells. The glycan expression on cell surface is a dynamic process associated with the cellular condition and status and reflects the pathophysiological steps of the morbid state.[8] The glycans of N-linked glycosylation (N-glycan) which share a common penta-saccharide core structure of Manα1−6(Manα1−3)Manβ1−4GlcNAcβ1−4GlcNAc have the ability to interfere with biomolecule interactions; thus they regulate many physiological events such as tumor progression.[2,9−13] For example, dynamic changes of β1.6GlcNAc-branched N-glycans on epidermal growth factor were observed to be associated with Mgat5 expression which influences cell motility and tumor metastasis.[14] The variational expression of cell surface mannose within N-glycan was also observed in the processes of tumorigenesis, brain aging, and differentiation.[13] As a result, the dynamic analysis of cell surface N-glycans is primarily significant to give insight into their roles in disease development and clinical diagnostics.

A series of methods, such as high-performance liquid chromatography (HPLC),[15] mass spectrometry (MS),[16] nuclear magnetic resonance (NMR),[17] and capillary electrophoresis (CE),[18] have been applied for glycomic analysis. Although some of these analyses are powerful enough to provide detailed structure information, they are not suitable to the *in situ* glycan analysis of living cells due to their destructive procedures and are time-consuming with complicated sample preparation and sophisticated instrumentation and most

Received: June 1, 2015
Accepted: September 3, 2015

DOI: 10.1021/acs.analchem.5b02048
Anal. Chem. XXXX, XXX, XXX−XXX

importantly incapable of profiling surface glycans in living cells due to their destructive procedures. Recently, there has been a rapid development in glycan analysis benefitted by the establishment of glyco-biosensors such as lectin arrays[19] and electrochemical biosensors[20−22] based on lectins, which can partially complement the limitations with potential applications for simple and dynamic analysis of carbohydrates on cell surfaces.

Electrogenerated chemiluminescence (ECL) involves a light emission process in a redox reaction of electrogenerated reactants. Compared to the conventional electrochemical and luminescence methods, the ECL technique not only presents high sensitivity and wide dynamic concentration response range but also is potential- and spatial-controlled.[23−25] The ECL biosensor has been widely applied in immunoassays,[26] DNA analysis,[27] and clinical diagnosis.[28−32] On the basis of the interaction of carbohydrates and lectins, ECL carbohydrate biosensors have also been developed for dynamic cell surface carbohydrates analysis by coupling the nanostructure bio-interfaces and ECL probes such as quantum dots, $Ru(bpy)_3^{2+}$ encapsulated silica spheres, and so on.[33−38] However, these approaches suffered from limited cell capture efficiency, low availability, and annoying cell counting procedures before analysis, which may cause false results, especially in complex biological matrix.

Recently, much attention has been centered on the single layer two-dimensional nanomaterials, such as graphene, MoS_2, and so on, owing to their fascinating two-dimensional structure, unusual electrochemical properties, large accessible surface area, and good biocompatibility. Graphitic carbon nitride (g-C_3N_4), a graphite-like layered material, has been verified to be an efficient and promising luminophore for ECL biosensors, which possesses the fascinating properties of low cost, good biocompatibility, and high chemical stability.[39] Moreover, the nanoscale of g-C_3N_4, such as g-C_3N_4 nanosheets, exhibits excellent water solubility and large surface area. The unique properties of the g-C_3N_4 nanosheet make it fascinating in ECL sensor fabrication for metallic ions,[40] dopamine,[41,42] and cancer biomarker detection.[43−46]

In this work, a dual-potential responsive electrogenerated chemiluminescence (ECL) biosensor was fabricated for synchronous detection of cancer cells and their surface N-glycan using $Ru(phen)_3^{2+}$ and gold-nanoparticle-modified g-C_3N_4 as the ECL probes at positive and negative potentials, respectively. Capture DNA hybridized aptamers intercalated with $Ru(phen)_3^{2+}$ ECL probes[47−49] were first immobilized on an electrochemical reduced MoS_2-nanosheet-modified electrode. The excellent electrochemical properties and large surfaces of MoS_2 improved the electron transfer rate and enhanced the cell capture efficiency on the electrode interface. In the presence of target cells, the capture DNA and $Ru(phen)_3^{2+}$ were released from the electrode interface owing to the specific interaction between cancer cells and the aptamer. Meanwhile, concanavalin A (Con A) conjugated gold-nanoparticle-modified graphite-C_3N_4 (Con A@Au−C_3N_4) was applied for the cell surface N-glycan evaluation owing to the excellent ECL properties of g-C_3N_4 at a negative potential. Thus, the cytosensing and cell surface N-glycan evaluation can be simultaneously realized with high sensitivity and excellent selectivity based on the ratio of the ECL intensity between the negative potential and positive potential ($\Delta ECL_n/\Delta ECL_p$), avoiding the traditional routing cell counting procedures. Moreover, the aptamer modified electrode can be regenerated for cyclic utilization by incubating in the capture DNA solutions. The ECL cytosensor exhibits excellent performances for the analysis of MCF-7 cancer cells and its surface N-glycan evaluation in human serum samples, which is sensitive to N-glycan inhibitors and can be applied for N-glycan inhibitor screening. The reusable and dual potential response ECL biosensor provides a feasibility tool to offer insight into the physiological functions of glycans in cellular processes as well as clinical diagnostics and drug screening.

EXPERIMENTAL SECTION

Reagents and Materials. Con A, $Ru(phen)_3Cl_2$, tunicamycin (TM), and polyacrylic acid (PAA) were purchased from Sigma-Aldrich. Tri-n-propylamine (TPA), 1-(3-(dimethylamino)propyl)-3-ethylcarbodiimide hydrochloride (EDC), and *N*-hydroxysuccinimide sodium salt (NHS) were obtained from Alfa Aesar. PNGase F was obtained from New England Biolabs Inc. (Ipswich, MA). $HAuCl_4{\cdot}3H_2O$ (48%, w/w) was obtained from Shanghai Reagent (Shanghai, China). The aptamer sequence was obtained from Shanghai Sangon Biological Engineering Technology & Services Co., Ltd. The sequence of the aptamer probe was 5′-NH_2-C_6H_{12}-CAC TAC AGA GGT TGC GTC CCA CGT TGT CCC ACG TTG TCA**TGG GGG GTT GGCCTG**-3′. The sequence of the complement DNA was 5′-**CAG GCC AAC CCC CCA**-3′. Other regents of analytical grade were obtained from Beijing Chemical Co. (Beijing, China)

Preparation of Layered MoS_2 Nanosheets. Intercalation and exfoliation of MoS_2 were prepared based on our recently developed method. Briefly, MoS_2 power was prepared by mixing the MoS_2 powder with melamine (with mole ratio of 1:3), and the mixed grind had added to it the appropriate *N*-methylpyrrolidone (NMP) as a lapping compound. The resulting slurry was then put into an alumina crucible, following heating to 700 °C in a tube furnace in an Ar atmosphere. The further deamination treatment was performed at 700 °C for 3 h.

Fabrication of Con A@Au-C_3N_4 Nanoprobes. The ECL nanoprobe Con A@Au-C_3N_4 was prepared by adding 40 μL of 0.02 mg mL^{-1} Con A solution to 120 μL of 2 mg mL^{-1}Au-C_3N_4 solution (Supporting Information). The mixture was incubated for 60 min at room temperature with gentle stirring and was centrifuged to remove extra Con A and redispersed in PBS solution. Finally, the solution was centrifuged at 5000 rpm, and the precipitant was redispersed in 120 μL of PBS solutions containing 1 mM Ca^{2+} and 1 mM Mn^{2+} to obtain the ECL nanoprobe Con A@Au-C_3N_4 solution.

Biosensor Preparation and Cell Capture. A glassy carbon electrode (GCE, diameter of 3 mm) was successively polished with 0.3 and 0.05 μm α-Al_2O_3 power followed by cleaning with distilled water and ethanol under ultrasonication. After being dried with nitrogen gas, 5 μL of a suspension solution of 0.5% PAA solution with 0.5 mg mL^{-1} MoS_2 was dropped onto the pretreated GCE and followed by an electrochemical reduction to yield the rMoS_2/PAA modified GCE (rMoS_2-PAA/GCE). Then, the electrode was immersed in 40 μL of a mixture solution containing 400 mM EDC and 100 mM NHS at 37 °C for 1 h. The immobilization of the aptamer was accomplished by incubating the rMoS_2-PAA/GCE electrode in 40 μL of 1 μM aptamer solution at 37 °C for 1 h. Thereafter, the washed electrode was immersed in ethanolamine for 15 min at 37 °C to block the excess active groups on the surface. Then, the above aptamer modified GCE was

DOI: 10.1021/acs.analchem.5b02048
Anal. Chem. XXXX, XXX, XXX−XXX

Scheme 1. Schematic Illustration of ECL Biosensor for Carbohydrate Expression on Cell Surface[a]

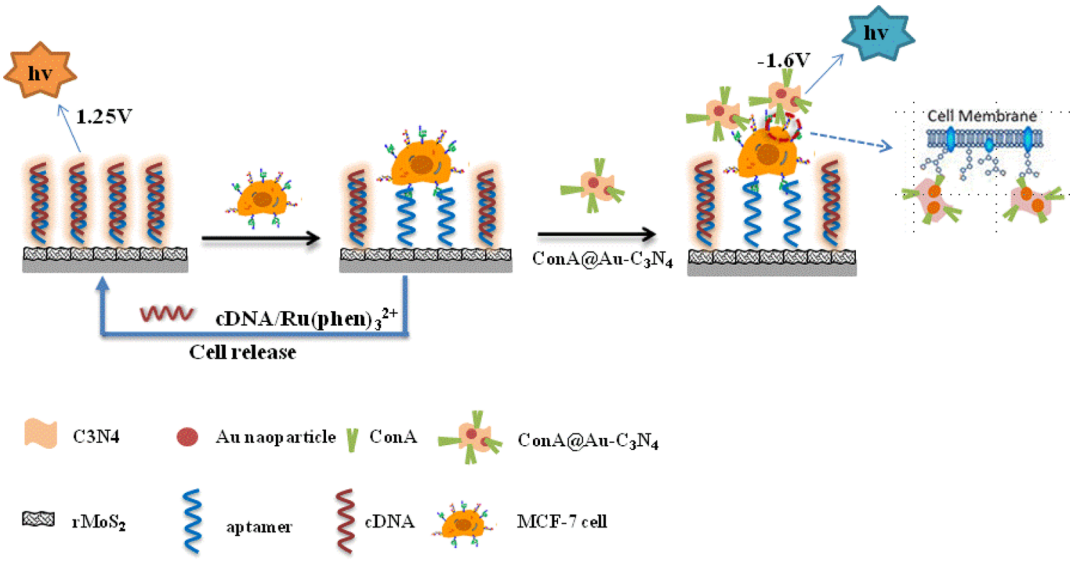

[a]The sandwich-type ECL biosensor for cell assay based on Con A@Au−C_3N_4.

immersed in 1 μM cDNA solution at 37 °C to form a DNA duplex on the surface. The resulted electrode was incubated in 20 mM Ru(phen)$_3^{2+}$ solution at 4 °C overnight to insert the Ru complex into the DNA duplex helix. After rinsing with PBS, the Ru(phen)$_3^{2+}$-inserted DNA duplex modified electrode (Ru(phen)$_3^{2+}$/cDNA/aptamer/rMoS$_2$-PAA/GCE) was ready for use. MCF-7 cell capture was performed by immersing the above electrode in 100 μL of MCF-7 cell suspension at certain concentrations. Finally, the cell captured electrode (cell/Ru(phen)$_3^{2+}$/cDNA/aptamer/rMoS$_2$−PAA/GCE) was carefully rinsed with PBS and used for subsequent ECL characterization.

ECL Cytosensing and Cell Surface N-glycan Evaluation. The cell captured electrode was incubated with 40 μL of the Con A@Au−C_3N_4 nanoprobe for 1 h at 37 °C and then was rinsed with PBS solution. Finally, a sandwich-type Con A@Au-C_3N_4/cell/Ru(phen)$_3^{2+}$/cDNA/aptamer/rMoS$_2$-PAA/GCE electrode was completed. For Ru(phen)$_3^{2+}$ associated positive-potential ECL analysis, the potential was scanned from 0.2 to 1.25 V in the PBS solution (pH 7.4, 100 mM) with 20 mM TPA. For Con A@Au-C_3N_4 probe associated negative-potential ECL analysis, it was performed by scanning from −1.6 V to 0 V in the PBS solution (pH 7.4, 100 mM) with 20 mM $S_2O_8^{2-}$.

Apparatus and Characterization. Transmission electron microscope (TEM) images were obtained with an H-7650B transmission electron microscope (Hitachi, Japan) opened at an accelerating voltage of 100 kV. UV−vis spectra were performed with a UV-3900 spectrophotometer (Hitachi, Japan). The cyclic voltammetry (CV) was conducted on a CHI660b instrument (CH Instrument Co., USA). Electrochemical impedance spectroscopy (EIS) was performed on a PARSTAT 2273 potentiostat/galvanostat (Advanced Measurement Technology Inc., USA) by applying an AC voltage amplitude of 5 mV in a frequency range from 0.01 Hz to 10^5 Hz in a 5 mM $K_3[Fe(CN)_6]/K_4[Fe(CN)_6]$ redox probe solution with 0.5 M KCl. The ECL measurements were carried out on an MPI-B multifunctional electrochemical analytical system (Xi'an Remex Analytical Instrument Ltd. Co., China). The voltage of the photomultiplier tube (PMT) was maintained at 600 V.

RESULTS AND DISCUSSION

The Regenerated and Dual Potential ECL Strategy for Cytosensing and Cell Surface N-glycan Evaluation. Scheme 1 shows the principle of the reusable and dual potential ECL biosensor for cell detection and cell surface N-glycan evaluation. MoS_2/PAA was first coated onto the surface of GCE in order to provide plenty of active sites for the immobilization of the SYL3C aptamer, which has strong affinity with EpCAM-positive cells.[50] In addition, the composite layer also improved the electron transfer rate on the electrode interface. After the intercalation of Ru(phen)$_3^{2+}$ in the grooves of hybridized DNA, a positive-potential ECL response was obtained, and it was decreased after the capture of cells because of the ds-DNA dissociation and Ru(phen)$_3^{2+}$ release. The changes of the ECL signal intensity at positive potential was associated with the numbers of the cells competitively adsorbed on the electrode. After the cells were captured, the electrodes were incubated in the solution with Con A@Au-C_3N_4 nanoprobes to form a sandwich type system based on the specific recognition between Con A and mannose or trimannoside; the core oligosaccharide of N-glycan on the cell surface and the ECL signals of Con A@Au-C_3N_4 nanoprobes at negative potential were recorded, which was associated with both the numbers of the cells and their surface glycans. As a result, multiple responsive signals were obtained through potential scanning, and the ratio of the ECL signal intensity of negative potential to that of positive potential ($\Delta ECL_{neg}/\Delta ECL_{pos}$) could accurately and directly exhibit N-glycan expression, excluding the artificial errors and troublesome cell counting procedures in a conventional one-channel signal assay. In addition, the aptamer modified electrode could be regenerated for cyclic utilization by incubating the cell captured electrode in the solution with capture DNA, which provided a simple, reusable, and multifunctional sensing platform for cytosensing and their surface N-glycan evaluation as well as clinical diagnosis and drug screening.

Electrochemical Characterization of MoS_2 Modified Electrode. MoS_2, a novel 2D nanomaterial, has been widely used in biosensing systems owing to its remarkable electron

DOI: 10.1021/acs.analchem.5b02048
Anal. Chem. XXXX, XXX, XXX−XXX

mobility and high density of electronic states.[51] Figure S3A shows the CV patterns of MoS_2−PAA/GCE from 0.6 V to −0.6 V measured in 0.5 M NaCl solution saturated with N_2. A reduction peak at −0.32 V was observed in the first cycle, which might be ascribed to the phase transition from the octahedral $1TMoS_2$ structure to the original trigonal-prismatic $2HMoS_2$ structure,[52] and it disappeared in the following potential scanning. The electron transfer on the electrode interface is sensitive to the surface microstructures, edge plane defects, and density of electronic states. Figure S3B displays the CV responses to the $Fe(CN)_6^{4-/3-}$ redox couple on the modified electrodes. The bare GCE exhibited a pair of well-defined redox peaks with a peak-to-peak potential separation (ΔE_p) of ∼75 mV. After functionalization with the low conductive PAA, the modified GCE, namely PAA/GCE electrode, shows an obvious decrease in the amperometric signal with a ΔE_p of ∼141 mV. When the MoS_2 was added to PAA, the peak currents in the CV were slightly increased and ΔE_p decreased to about 91 mV. After the electrochemical treatment of MoS_2 ($rMoS_2$), a peak potential gap of ∼79 mV was obtained, which was similar to that of bare GCE, indicating the excellent electron transfer ability of $rMoS_2$ and great promise in electrochemical sensing applications.

Electrochemical Characterizations of the Biosensor. CV and EIS are effective and facile electrochemical techniques for monitoring the changes in the surface features of the modified electrodes in the assembly processes. Figure 1A displays the CV curves of the step by step modified GCE using $Fe(CN)_6^{4-/3-}$ as electroactive probes. The $rMoS_2$-PAA/GCE exhibited a couple of reversible redox peaks and intensive peak current in curve a, attributing to the large surface and excellent conductivity of $rMoS_2$. When the aptamer was immobilized onto the above electrode, an obvious decrease in the amperometric signal was found (curve b). The peak currents in the CV were gradually decreased after the hybridization of complementary capture DNA and intercalation of $Ru(phen)_3^{2+}$ (curve c). The gap between the anodic and cathodic peaks became wider after subsequent capture of MCF-7 cells by the specific binding between aptamer and cells (curve d). This phenomenon was ascribed to the electronically inert feature of DNA and cell that blocked the electron transfer and mass transfer of $Fe(CN)_6^{4-/3-}$ ions at the electrode surface. Finally, the biosensor was incubated with the nanoprobe of Con A@Au-C_3N_4. As seen in curve e, the binding of nanoprobes still led to a slight decrease in peak currents which might be resulted from the bad conductivity of the nanoprobes.

The Nyquist plot consists of a semicircle part at a higher frequency range and a straight linear part at a lower frequency range. As seen in Figure 1B, the diameter of the semicircle which equals the electron transfer resistance (Ret) at the electrode interface increases successively with sequential assembly of the aptamer (curve b), capture of the cell (curve d), and incubation of nanoprobes (curve e), indicating an enhancement of the Ret step by step. These results are in conformity with the phenomena in CVs, demonstrating the successful assembly of the biosensor.

Optimization of the Experimental Conditions. The effect of cell incubation time, probe incubation time, and the ratio of Au−C_3N_4 to Con A on the performances of the ECL biosensor were investigated. The optimal volume ratio of Au-C_3N_4 (2 mg mL^{-1}) to Con A (0.02 mg mL^{-1}) was 3:1 for the preparation of the ECL nanoprobe (Figure S5A). The incubation time for cell capture is crucial for the ECL

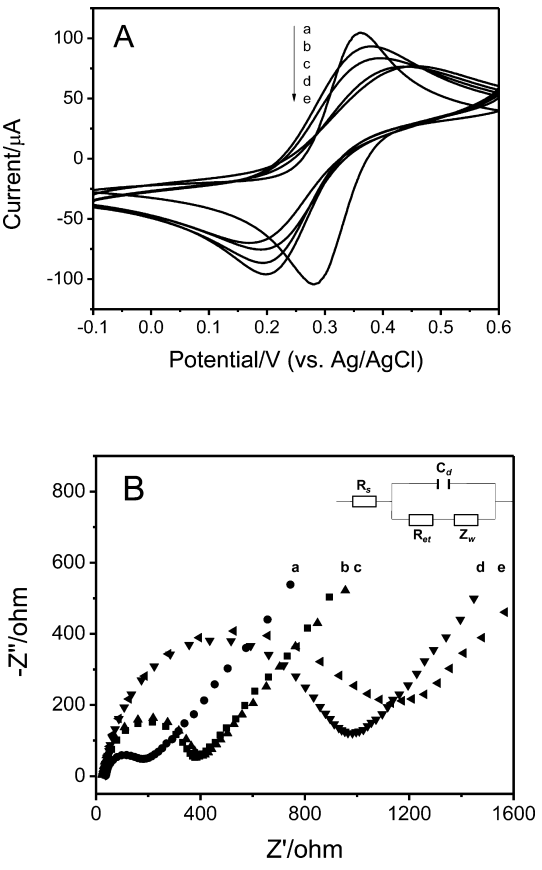

Figure 1. Cyclic voltammograms (A) and electrochemical impedance spectra (B) of (a) $rMoS_2$-PAA/GCE, (b) aptamer/$rMoS_2$-PAA/GCE, (c) cDNA/ethanolamine/aptamer/$rMoS_2$-PAA/GCE, (d) cell/Ru-$(phen)_3^{2+}$/cDNA/ethanolamine/aptamer/$rMoS_2$-PAA/GCE, (e) Con A@Au-C_3N_4/cell/$Ru(phen)_3^{2+}$/cDNA/ethanolamine/aptamer/$rMoS_2$-PAA/GCE. The electrolyte solution is 5 mM $K_4Fe(CN)_6$ and 5 mM $K_3Fe(CN)_6$ containing 0.5 M KCl. The scan rate is 100 mV s^{-1}. The impedance spectra frequency is 0.1−10^5 Hz, and the amplitude is 10 mV. The inset is the equivalent circuit of Faradaic electrochemical impedance spectra.

cytosensing. The ECL intensity at a positive potential as a function of incubation time was shown in Figure S5B. The ECL intensity of the biosensor increased with the increasing incubation time and then reached a plateau at 60 min. As a result, the cell incubation time of 60 min was used in the following experiments. The ECL performance of the biosensor was also closely related to the incubation time for Con A@Au−C_3N_4 adsorption. After incubating with MCF-7 cell suspension for 60 min, it can be seen that the ECL value increased when the nanoprobe incubation time increased, and it leveled off after incubation for 60 min (Figure S5C, Supporting Information). Meanwhile, as shown in Figure S5D (Supporting Information), with the increasing volume of nanoprobe (approximately 2 mg mL^{-1}) solution, the ECL response was significantly increased from 3 to 13 μL, while an insignificant difference was observed for greater volumes. Therefore, the optimal conditions for the biosensor were 60 min for cell capture and 60 min and 10 μL for nanoprobe incubation.

ECL Behaviors of the Biosensor. In this strategy, the ECL responses from both $Ru(phen)_3^{2+}$ and Con A@Au-C_3N_4 nanoprobes were closely related with the cells captured on the electrode. In addition, the Con A@Au-C_3N_4 nanoprobes were adsorbed on the cell surface based on the specific

DOI: 10.1021/acs.analchem.5b02048
Anal. Chem. XXXX, XXX, XXX−XXX

interaction between the mannose and Con A. Thus, the ECL response at negative potential from Con A@Au-C_3N_4 nanoprobes could be applied for the evaluation of the mannose core in N-glycan. As a result, the simultaneously cytosensing and dynamic cell surface N-Glycan evaluation could be realized by the potential scanning. The ECL behavior of the biosensor at positive potential was first investigated in 0.1 M PBS with 20 mM TPA. The $Ru(phen)_3^{2+}$/cDNA/aptamer/$rMoS_2$-PAA/GCE presented a strong ECL signal at 1.2 V, confirming the successful intercalation of $Ru(phen)_3^{2+}$ into the grooves of ds-DNA (Figure 2A). While the $Ru(phen)_3^{2+}$/cDNA/aptamer/

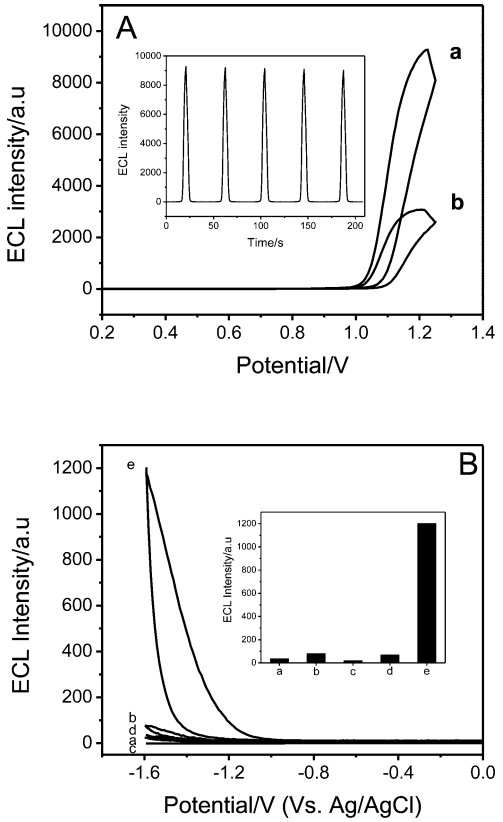

Figure 2. (A) ECL intensity−potential behavior of (a) $Ru(phen)_3^{2+}$/cDNA/ethanolamine/aptamer/$rMoS_2$-PAA/GCE, (b) cell/$Ru(phen)_3^{2+}$/cDNA/ethanolamine/aptamer/$rMoS_2$-PAA/GCE in 0.1 M PBS (pH 7.4) containing 20 mM TPA. The scan rate is 50 mV/s. The inset is the ECL−time curve of $Ru(phen)_3^{2+}$/cDNA/ethanolamine/aptamer/$rMoS_2$-PAA/GCE in 0.1 M PBS (pH 7.4) containing 20 mM TPA under continuous CVs for five cycles. The PMT voltage is 600 V. The potential is 0.2−1.25 V (vs Ag/AgCl). (B) ECL intensity−potential behavior of (a) Con A@Au-C_3N_4/cell/$rMoS_2$-PAA/GCE, (b) Con A@Au-C_3N_4/aptamer/$rMoS_2$-PAA/GCE, (c) cell/rMoS-PAA/GCE, (d) Con A@Au-C_3N_4/$rMoS_2$-PAA/GCE, and (e) Con A@Au-C_3N_4/cell/aptamer/$rMoS_2$-PAA/GCE in 0.1 M PBS (pH 7.4) containing 20 mM $K_2S_2O_8$. The scan rate is 100 mV s^{-1}. The PMT voltage is 600 V. The potential is −1.6 to ~0 V (vs Ag/AgCl). The concentration of MCF-7 cells is 5.0×10^5 cells mL^{-1}.

$rMoS_2$-PAA/GCE electrode was immersed in cancer cell solutions, the ECL signal was sharply decreased because of the specific recognition between the aptamer and cells. As a result, the capture DNA and intercalated $Ru(phen)_3^{2+}$ were released from the electrode surface.

The negative ECL behavior of the biosensor from Con A@Au-C_3N_4 nanoprobes was also investigated in 0.1 M PBS with 20 mM $S_2O_8^{2-}$. Figure 2B shows the ECL response as a function of potential. As can be seen in curve e, the Con A@Au-C_3N_4/cell/aptamer/$rMoS_2$-PAA/GCE exhibited a strong ECL emission at −1.6 V, confirming the specific recognition of the Con A@Au-C_3N_4 nanoprobes with the cells.

A series of control experiments was performed by the ECL measurement to verify feasibility of the biosensor. As shown in Figure 2B, the $rMoS_2$-PAA/GCE without aptamer immobilization showed a quiet, low ECL signal, whenever it was followed by incubating with a nanoprobe or both cell and nanoprobe (curves d and a). In addition, aptamer/$rMoS_2$-PAA/GCE without incubating with cells showed slight ECL emission (curve b), which indicated that only slight amounts of nanoprobe were absorbed on it. Moreover, the electrode cell/aptamer/$rMoS_2$-PAA/GCE without incubation of ECL nanoprobes gave the lowest response (curve c), which demonstrated that the ECL signal was originated from the nanoprobe. These results indicated that the nonspecific adsorption was very weak. Comparatively, the well-prepared biosensor under all procedures exhibited strong ECL intensity (curve e). This suggested that the aptamer had strong affinity with the cell, and Con A could well recognize the mannose and trimannoside on the cell surface and capture the cells. Thus, the as-proposed biosensor was sensitive and feasible.

Cytosensing of the Biosensor. On the basis of the optimal conditions, the determination of MCF-7 cells was applied at both positive scanning and negative scanning. Figure 3 displays the positive ECL signal of the biosensor from $Ru(phen)_3^{2+}$ at different concentrations of MCF-7 cells. It was observed that the ECL signal intensity decreased with increased cell concentration, and it was linear with the logarithm of the concentration of MCF-7 cells in the range from 10^2 to 10^6. The detection limit (3σ) was 150 cells mL^{-1}. Taking into account that 100 μL of the MCF-7 cell suspension was used for incubation, the ECL strategy achieved the limit of detection of only 15 MCF-7 cells. The high sensitivity could be ascribed to the multivalent effect of the aptamer conjugated nanostructured interface that we had reported.[36,53] In addition, the negative ECL signals from Con A@Au-C_3N_4 nanoprobes of the biosensor were also measured at different concentrations of MCF-7 cells (Figure S6 in the Supporting Information). The negative ECL signal intensity increased with the increased MCF-7 cell numbers, and a similar linear relationship between the ECL intensity and with the logarithm of the concentration of MCF-7 cells was obtained. The facts demonstrated that both the ECL signals from $Ru(phen)_3^{2+}$ and Con A@Au-C_3N_4 nanoprobes could be applied for sensitive cell detection.

In addition, the selectivity of the ECL biosensor was also studied by incubating the $Ru(phen)_3^{2+}$/cDNA/aptamer/$rMoS_2$-PAA/GCE in the solution with different cell lines such as MCF-7, K562, 293T, and Hela cells. As shown in Figure 4A, there were remarkable ECL signal changes (ΔECL) when the electrode was immersed in the MCF-7 cell solution. Minimal ECL signal changes were observed in the solution with K562, 293T, and Hela cells. The facts demonstrated that the as designed ECL biosensor possessed excellent selectivity. Moreover, the selectivity of the biosensor was also confirmed by incubating the $Ru(phen)_3^{2+}$/cDNA/aptamer/$rMoS_2$-PAA/GCE electrode in the K562 cell solution with various concentrations of MCF-7 cells. The ECL signal changes were shown in Figure 4B. It was obvious that the ECL signal changes increased with the increased numbers ratios of MCF-7 cells to K562 cells and were similar to the results from solution merely

DOI: 10.1021/acs.analchem.5b02048
Anal. Chem. XXXX, XXX, XXX−XXX

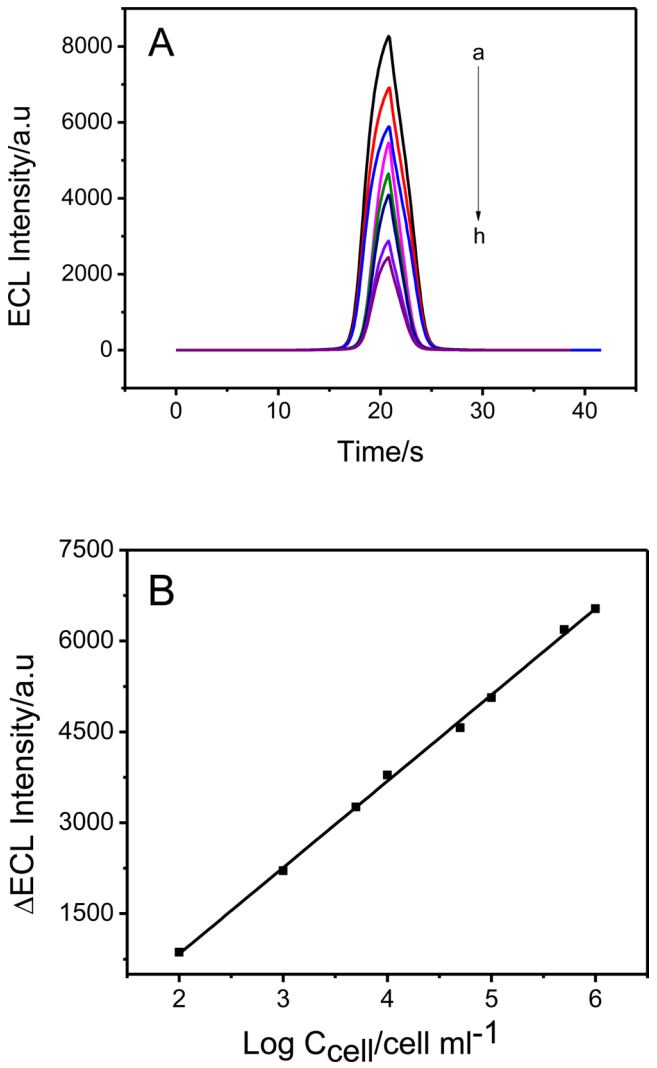

Figure 3. (A) The ECL intensities of positive assay versus different MCF-7 cell concentrations (from a to f was 1.0×10^2, 1.0×10^3, 5.0×10^3, 1.0×10^4, 5.0×10^4, 1.0×10^5, 5.0×10^5, and 1.0×10^6 cells mL^{-1}, respectively) in 0.1 M PBS (pH 7.4). The PMT voltage is 600 V. (B) Plots of positive ECL intensity vs logarithm value of MCF-7 cell concentration.

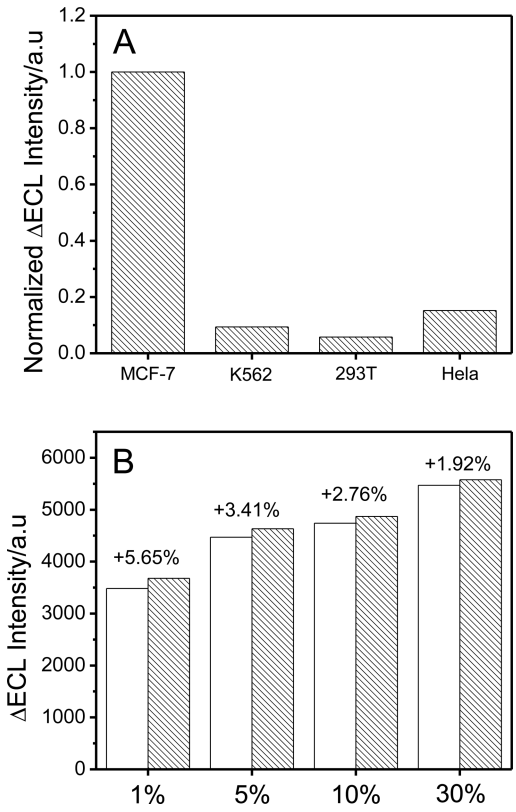

Figure 4. (A) Normalized ECL intensity of the biosensor from the solution with different cell lines at a concentration of 5.0×10^5 cells mL^{-1}. (B) Selective recognition of MCF-7 cells in mixed cell samples in cell media. Cell mixture samples containing MCF-7 and K562 cells were prepared with different percentages of MCF-7 cells (1%, 5%, 10%, 30%, respectively) with a 5×10^4 total cell number in 100 μL of cell media.

with MCF-7 cells. The maximal error of ΔECL between the MCF-7 cell solution and the mixture of MCF-7 and K562 cell was calculated to be 5.62% when the content of MCF-7 in the mixture was 1%, and it gradually decreased to be 1.92% when the MCF-7 content increased. These results demonstrated that the as designed biosensor could effectively differentiate the target cells from the cell mixture, which held considerable potential for simple, rapid, and specific cancer cell detection in clinical samples.

Evaluating Cell Surface N-Glycan Expression under the External Stimuli of Inhibitors and Enzyme. N-glycans have essential roles in diverse biological processes. In this strategy, the negative signals from Con A@Au-C_3N_4 nanoprobes are associated with both cell concentration and N-glycan expression, and the positive ECL signal comes from the cell captured. Thus, the ratio of ECL intensity from the negative and positive potential signals ($\Delta ECL_n/\Delta ECL_p$) can be applied for the dynamic evolution of the N-glycan expression on the cell surface, which can avoid the additional cell counting procedures and excludes the artificial errors and troublesome cell counting procedures in a complex biological matrix. To demonstrate the pattern, cell surface N-glycan expression of MCF-7 was analyzed with the ECL biosensor under the treatment of TM, an inhibitor for N-glycan expression by blocking the first step in the biosynthesis of N-glycosylation in cells.[54] A progressive decrease in the ECL intensity changes can be observed when collating the TM-treated cells with untreated cells in Figure 5. After 48 h of treatment, the ECL signal change was 45.3%. The decreased ECL response of cell surface N-glycan expression was caused by TM, which can inhibit N-glycan expression. In addition, enzymatic cleavage and release of N-glycans from asparagines was performed by PNGase F,[55] an amidase that cleaves between the innermost GlcNAc and asparagine residues of N-linked proteins. Compared with that of untreated cells, the ECL intensity of PNGase F-treated cells was sharply dropped to 37.3% and was at the same level after enzymatic digestion with the treatments with TM. As a result, the proposed ECL biosensor was able to be applied for cell surface N-glycan evaluation. It was demonstrated that the constructed biosensor could dynamically evaluate cell surface N-glycan expression with high sensitivity.

It is important that both of the ECL signals at positive potential and negative potential are closely related with the cells captured on the electrode. As a result, the ratio of ECL intensity from the negative and positive potential signals ($\Delta ECL_n/\Delta ECL_p$) is independent from cell concentration. To demon-

DOI: 10.1021/acs.analchem.5b02048
Anal. Chem. XXXX, XXX, XXX−XXX

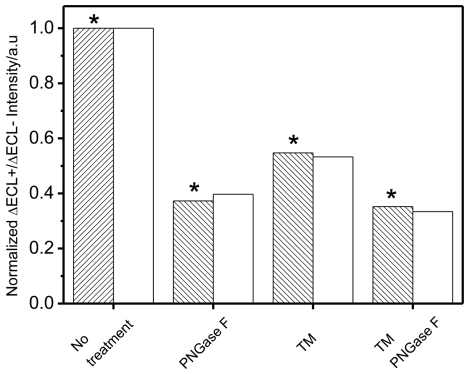

Figure 5. N-Glycan expression of MCF-7 cell surface without or with treatment of PNGase F for 24 h and after incubation with TM (1 mg mL^{-1}) for 48 h. The positive ECL peak intensity was obtained at 1.2 V (vs Ag/AgCl) in 0.1 M PBS (pH 7.4) containing 20 mM TPA, while the negative ECL peak intensity was obtained at −1.6 V in 0.1 M PBS containing 20 mM $S_2O_8^{2-}$. The PMT voltage is 600 V. The gray bars (*) and the white bars representing the MCF-7 cell concentration is 5 × 10^5 cells $mL^{-1}$and 5 × 10^4 cells mL^{-1}, respectively.

strate the validity, the same cell lines (MCF-7) with different concentrations of cell concentration were treated with TM and PNGase F under the same conditions. The $\Delta ECL_n/\Delta ECL_p$ signal change of the TM-treated cells and PNGase F-treated cells with a concentration of 5 × 10^4 cells mL^{-1} was 46.7% and 60.3%, respectively. The change of $\Delta ECL_n/\Delta ECL_p$ was similar to that of cells at a counted concentration of 5 × 10^5 cells mL^{-1}, which indicated that cell numbers had no influence on the $\Delta ECL_n/\Delta ECL_p$ value. Thus, the as prepared ECL biosensor could be used for evaluation of cell surface N-glycan expression excluding the traditional cell counting procedures that avoid the individual error in the experiments.

Reusability of the Biosensor. In this strategy, the competitive adsorption of the cDNA and cancer cell takes place on the aptamer modified electrode interface. The free energies of the competition reaction are associated with the change in the ratio of the concentration of the products to the reactants, which could be described by the following equation: $\Delta G = \Delta G^\circ + RT \ln Q$, where Q is the reaction quotient. As a result, the large ratio value C_{cDNA}/C_{cells} makes the reaction leave the standard state and shift to the reversible side to reach equilibrium, and cells are released from the electrode. Therefore, the cDNA/aptamer/$rMoS_2$-PAA/GCE can be regenerated from cells/aptamer/$rMoS_2$-PAA/GCE by being incubated in the cDNA solution. Figure 6A shows the Nyquist patterns of cells/aptamer/$rMoS_2$-PAA/GCE treated without (curve a) and with cDNA (curve b). After incubating in cDNA solution, the diameter of the semicircle of cells/aptamer/$rMoS_2$-PAA/GCE in the Nyquist curve decreased and was similar to that of cDNA/aptamer/$rMoS_2$-PAA/GCE without any treatment. The results indicated that the adhered cells were almost completely released. The regeneration of the biosensor was also characterized by the ECL behaviors of the $Ru(phen)_3^{2+}$ chelated cDNA/aptamer/$rMoS_2$-PAA/GCE. As presented in Figure 6B, when the $Ru(phen)_3^{2+}$/cDNA/aptamer/$rMoS_2$-PAA/GCE electrode was immersed in cancer cell solutions, the ECL signal was sharply decreased. After incubating in cDNA solution and intercalating with $Ru(phen)_3^{2+}$, the ECL intensity almost regained its initial value. These cell attachment and detachment procedures were repeated for several times. The as prepared biosensor can

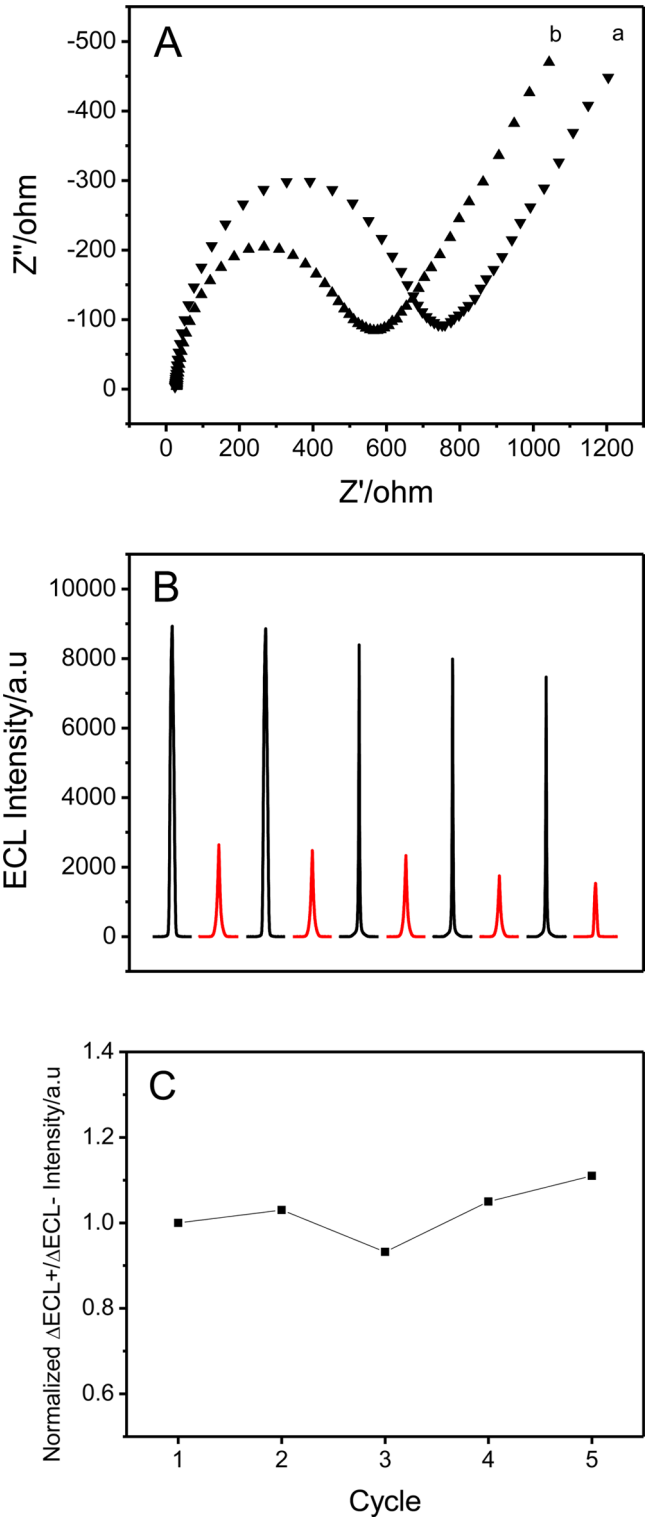

Figure 6. (A) Electrochemical impedance spectra of cell/$Ru(phen)_3^{2+}$/cDNA/aptamer/$rMoS_2$-PAA/GCE before (a) and after (b) treatment with cDNA. (B) Positive ECL intensity of the cell detachment (black line) and attachment (red line) from the first time to the fifth time. (C) The ratio of ECL intensity from the negative and positive potential signals ($\Delta ECL_n/\Delta ECL_p$) from the first time to the fifth time. The cell concentration is 5.0 × 10^5 cells mL^{-1}.

also be applied for repeatable analysis of cell surface N-glycan as shown in Figure 6C. The $\Delta ECL_n/\Delta ECL_p$ nearly kept a stable value after several cycles. Such a sensitive and reusable ECL

DOI: 10.1021/acs.analchem.5b02048
Anal. Chem. XXXX, XXX, XXX−XXX

biosensor shows great promise for dynamic evaluation of cell surface N-glycan expression and drug screening.

CONCLUSIONS

A reusable and dual-potential ECL biosensor was fabricated for multiple cancer cell detection and *in situ* evaluation of cell surface glycan expression synchronously. In this work, the cytosensing and cell surface N-glycan evaluation could be simultaneously realized with high sensitivity and excellent selectivity based on the ratio of the ECL intensity between the negative potential and positive potential ($\Delta ECL_n/\Delta ECL_p$), avoiding the traditional counting cell counting procedures. Thus, the strategy was successfully used to evaluate N-glycan expression of MCF-7 cell lines and the change of cell surface carbohydrates disturbed by the external stimuli of N-glycan inhibitor TM or released by PNGase F. Moreover, cyclic utilization of the electrode was realized by adding plenty of cDNA, which had the potential to be used in a microfluidic chip system. The novel strategy would contribute to the understanding of complex native glycan-related biological processes as well as serve as an impetus for elucidating the physiological processes of N-glycan-related diseases and clinical diagnostics.

ASSOCIATED CONTENT

Supporting Information

The Supporting Information is available free of charge on the ACS Publications website at DOI: 10.1021/acs.analchem.5b02048.

Figures S1−S6 (PDF)

AUTHOR INFORMATION

Corresponding Author

*Tel.: 86-10-62798187. Fax: 86-10-62771149. E-mail: liuyang@mail.tsinghua.edu.cn.

Notes

The authors declare no competing financial interest.

ACKNOWLEDGMENTS

This work was financially supported by the National Natural Science Foundation of China (No. 21375073, 21235004), National Basic Research Program of China (No. 2011CB935704, 2013CB934004), and Tsinghua University Initiative Scientific Research Program (2014z21027).

REFERENCES

(1) Pilobello, K. T.; Mahal, L. K. *Curr. Opin. Chem. Biol.* **2007**, *11*, 300−305.
(2) Dennis, J. W.; Nabi, I. R.; Demetriou, M. *Cell* **2009**, *139*, 1229−1241.
(3) Flanagan-Steet, H. R.; Steet, R. *Glycoconjugate J.* **2013**, *30*, 33−40.
(4) Gu, J. G.; Isaji, T.; Xu, Q. S.; Kariya, Y.; Gu, W.; Fukuda, T.; Du, Y. G. *Glycoconjugate J.* **2012**, *29*, 599−607.
(5) Haltiwanger, R. S.; Lowe, J. B. *Annu. Rev. Biochem.* **2004**, *73*, 491−537.
(6) Lau, K. S.; Dennis, J. W. *Glycobiology* **2008**, *18*, 750−760.
(7) Marth, J. D.; Grewal, P. K. *Nat. Rev. Immunol.* **2008**, *8*, 874−887.
(8) Fuster, M. M.; Esko, J. D. *Nat. Rev. Cancer* **2005**, *5*, 526−542.
(9) Marino, K.; Bones, J.; Kattla, J. J.; Rudd, P. M. *Nat. Chem. Biol.* **2010**, *6*, 713−723.
(10) Nakano, M.; Saldanha, R.; Gobel, A.; Kavallaris, M.; Packer, N. H. *Mol. Cell. Proteomics* **2011**, *10*, 12.
(11) Moremen, K. W.; Tiemeyer, M.; Nairn, A. V. *Nat. Rev. Mol. Cell Biol.* **2012**, *13*, 448−462.
(12) Morishima, S.; Morita, I.; Tokushima, T.; Kawashima, H.; Miyasaka, M.; Omura, K.; Murota, S. *J. Endocrinol.* **2003**, *176*, 285−292.
(13) Zhang, X. A.; Teng, Y. Q.; Fu, Y.; Xu, L. L.; Zhang, S. P.; He, B.; Wang, C. G.; Zhang, W. *Anal. Chem.* **2010**, *82*, 9455−9460.
(14) Cheung, P.; Pawling, J.; Partridge, E. A.; Sukhu, B.; Grynpas, M.; Dennis, J. W. *Glycobiology* **2007**, *17*, 828−837.
(15) Royle, L.; Campbell, M. P.; Radcliffe, C. M.; White, D. M.; Harvey, D. J.; Abrahams, J. L.; Kim, Y. G.; Henry, G. W.; Shadick, N. A.; Weinblatt, M. E.; Lee, D. M.; Rudd, P. M.; Dwek, R. A. *Anal. Biochem.* **2008**, *376*, 1−12.
(16) Nishikaze, T.; Kaneshiro, K.; Kawabata, S.; Tanaka, K. *Anal. Chem.* **2012**, *84*, 9453−9461.
(17) Carneiro, M. G.; Koharudin, L. M. I.; Ban, D.; Sabo, T. M.; Trigo-Mourino, P.; Mazur, A.; Griesinger, C.; Gronenborn, A. M.; Lee, D. *Angew. Chem., Int. Ed.* **2015**, *54*, 6462−6465.
(18) Vanderschaeghe, D.; Szekrenyes, A.; Wenz, C.; Gassmann, M.; Naik, N.; Bynum, M.; Yin, H. F.; Delanghe, J.; Guttman, A.; Callewaert, N. *Anal. Chem.* **2010**, *82*, 7408−7415.
(19) Chen, S. Y.; Zheng, T.; Shortreed, M. R.; Alexander, C.; Smith, L. M. *Anal. Chem.* **2007**, *79*, 5698−5702.
(20) Cheng, W.; Ding, L.; Ding, S. J.; Yin, Y. B.; Ju, H. X. *Angew. Chem., Int. Ed.* **2009**, *48*, 6465−6468.
(21) Ding, L.; Ji, Q. J.; Qian, R. C.; Cheng, W.; Ju, H. X. *Anal. Chem.* **2010**, *82*, 1292−1298.
(22) Bertok, T.; Klukova, L.; Sediva, A.; Kasak, P.; Semak, V.; Micusik, M.; Omastova, M.; Chovanova, L.; Vlcek, M.; Imrich, R.; Vikartovska, A.; Tkac, J. *Anal. Chem.* **2013**, *85*, 7324−7332.
(23) Richter, M. M. *Chem. Rev.* **2004**, *104*, 3003−3036.
(24) Liu, Z.; Qi, W.; Xu, G. *Chem. Soc. Rev.* **2015**, *44*, 3117−3142.
(25) Wittmann, V.; Pieters, R. J. *Chem. Soc. Rev.* **2013**, *42*, 4492−4503.
(26) Duan, R. X.; Zhou, X. M.; Xing, D. *Anal. Chem.* **2010**, *82*, 3099−3103.
(27) Wang, Y.; Lu, J.; Tang, L. H.; Chang, H. X.; Li, J. H. *Anal. Chem.* **2009**, *81*, 9710−9715.
(28) Xu, S. J.; Liu, Y.; Wang, T. H.; Li, J. H. *Anal. Chem.* **2011**, *83*, 3817−3823.
(29) Han, F.; Jiang, H.; Fang, D.; Jiang, D. *Anal. Chem.* **2014**, *86*, 6896−6902.
(30) Liu, Z.; Zhang, W.; Hu, L.; Li, H.; Zhu, S.; Xu, G. *Chem. - Eur. J.* **2010**, *16*, 13356−13359.
(31) Zhang, H. R.; Wu, M. S.; Xu, J. J.; Chen, H. Y. *Anal. Chem.* **2014**, *86*, 3834−3840.
(32) Zhang, H. R.; Xu, J. J.; Chen, H. Y. *Anal. Chem.* **2013**, *85*, 5321−5325.
(33) Han, E.; Ding, L.; Jin, S.; Ju, H. X. *Biosens. Bioelectron.* **2011**, *26*, 2500−2505.
(34) Yang, H. Y.; Wang, Y. Q.; Qi, H. L.; Gao, Q.; Zhang, C. X. *Biosens. Bioelectron.* **2012**, *35*, 376−381.
(35) Zhang, J. J.; Ruo, Y.; Chen, S. H.; Zhong, X.; Wu, X. P. *RSC Adv.* **2014**, *4*, 48465−48471.
(36) Chen, X.; Wang, Y.; Zhang, Y.; Chen, Z.; Liu, Y.; Li, Z.; Li, J. *Anal. Chem.* **2014**, *86*, 4278−4286.
(37) Chen, Z.; Liu, Y.; Wang, Y.; Zhao, X.; Li, J. *Anal. Chem.* **2013**, *85*, 4431−4438.
(38) Wang, Y. Z.; Chen, Z. H.; Liu, Y.; Li, J. H. *Nanoscale* **2013**, *5*, 7349−7355.
(39) Zhao, Z.; Sun, Y.; Dong, F. *Nanoscale* **2015**, *7*, 15−37.
(40) Cheng, C. M.; Huang, Y.; Tian, X. Q.; Zheng, B. Z.; Li, Y.; Yuan, H. Y.; Xiao, D.; Xie, S. P.; Choi, M. M. F. *Anal. Chem.* **2012**, *84*, 4754−4759.
(41) Lu, Q. Y.; Zhang, J. J.; Liu, X. F.; Wu, Y. Y.; Yuan, R.; Chen, S. H. *Analyst* **2014**, *139*, 6556−6562.
(42) Liu, Y. T.; Wang, Q. B.; Lei, J. P.; Hao, Q.; Wang, W.; Ju, H. X. *Talanta* **2014**, *122*, 130−134.
(43) Chen, L.; Zeng, X.; Si, P.; Chen, Y.; Chi, Y.; Kim, D. H.; Chen, G. *Anal. Chem.* **2014**, *86*, 4188−4195.

DOI: 10.1021/acs.analchem.5b02048
Anal. Chem. XXXX, XXX, XXX−XXX

(44) Li, X. J.; Zhang, X. Y.; Ma, H. M.; Wu, D.; Zhang, Y.; Du, B.; Wei, Q. *Biosens. Bioelectron.* **2014**, *55*, 330−336.
(45) Han, T.; Li, X.; Li, Y.; Cao, W.; Wu, D.; Du, B.; Wei, Q. *Sens. Actuators, B* **2014**, *205*, 176−183.
(46) Li, X. J.; Guo, Z. K.; Li, J. X.; Zhang, Y.; Ma, H. M.; Pang, X. H.; Du, B.; Wei, Q. *Anal. Chim. Acta* **2015**, *854*, 40−46.
(47) Xu, X. H.; Yang, H. C.; Mallouk, T. E.; Bard, A. J. *J. Am. Chem. Soc.* **1994**, *116*, 8386−8387.
(48) Smolensky, E. D.; Peterson, K. L.; Weitz, E. A.; Lewandowski, C.; Pierre, V. C. *J. Am. Chem. Soc.* **2013**, *135*, 8966−8972.
(49) Yang, L.; Zhang, Y.; Li, R.; Lin, C.; Guo, L.; Qiu, B.; Lin, Z.; Chen, G. *Biosens. Bioelectron.* **2015**, *70*, 268−274.
(50) Song, Y.; Zhu, Z.; An, Y.; Zhang, W.; Zhang, H.; Liu, D.; Yu, C.; Duan, W.; Yang, C. J. *Anal. Chem.* **2013**, *85*, 4141−4149.
(51) Butler, S. Z.; Hollen, S. M.; Cao, L. Y.; Cui, Y.; Gupta, J. A.; Gutierrez, H. R.; Heinz, T. F.; Hong, S. S.; Huang, J. X.; Ismach, A. F.; Johnston-Halperin, E.; Kuno, M.; Plashnitsa, V. V.; Robinson, R. D.; Ruoff, R. S.; Salahuddin, S.; Shan, J.; Shi, L.; Spencer, M. G.; Terrones, M.; Windl, W.; Goldberger, J. E. *ACS Nano* **2013**, *7*, 2898−2926.
(52) Wu, S.; Zeng, Z.; He, Q.; Wang, Z.; Wang, S. J.; Du, Y.; Yin, Z.; Sun, X.; Chen, W.; Zhang, H. *Small* **2012**, *8*, 2264−2270.
(53) Chen, X.; He, Y.; Zhang, Y.; Liu, M.; Liu, Y.; Li, J. *Nanoscale* **2014**, *6*, 11196−11203.
(54) Elbein, A. D. *Annu. Rev. Biochem.* **1987**, *56*, 497−534.
(55) Tretter, V.; Altmann, F.; Marz, L. *Eur. J. Biochem.* **1991**, *199*, 647−652.

DOI: 10.1021/acs.analchem.5b02048
Anal. Chem. XXXX, XXX, XXX−XXX